

Wavelength-Scanned Surface-Enhanced Raman Excitation Spectroscopy

Adam D. McFarland,[†] Matthew A. Young,[†] Jon A. Dieringer, and Richard P. Van Duyne*

Department of Chemistry, Northwestern University, Evanston, Illinois 60208-3113

Received: January 28, 2005; In Final Form: April 8, 2005

A detailed wavelength-scanned surface-enhanced Raman excitation spectroscopy (WS SERES) study of benzenethiol adsorbed on Ag nanoparticle arrays, fabricated by nanosphere lithography (NSL), is presented. These NSL-derived Ag nanoparticle array surfaces are both structurally well-characterized and extremely uniform in size. The WS SERES spectra are correlated, both spatially and spectrally, with the corresponding localized surface plasmon resonance (LSPR) spectra of the nanoparticle arrays. The surface-enhanced Raman scattering (SERS) spectra were measured in two excitation wavelength ranges: (1) 425–505 nm, and (2) 610–800 nm, as well as with the 532-nm line from a solid-state diode-pumped laser. The WS SERES spectra have line shapes similar to those of the LSPR spectra. The maximum SERS enhancement factor is shown to occur for excitation wavelengths that are blue-shifted with respect to the LSPR λ_{max} of adsorbate-covered nanoparticle arrays. Three vibrational modes of benzenethiol (1575, 1081, and 1009 cm^{-1}) are studied simultaneously on one substrate, and it is demonstrated that the smaller Raman shifted peak shows a maximum enhancement closer to the LSPR λ_{max} than that of a larger Raman shifted peak. This is in agreement with the predictions of the electromagnetic (EM) enhancement mechanism of SERS. Enhancement factors of up to $\sim 10^8$ are achieved, which is also in good agreement with our previous SERES studies.

Introduction

Noble metal nanoparticles have gained widespread interest because of their application to chemical and biological sensing,^{1–5} optical device fabrication,^{6–8} and surface-enhanced spectroscopies.^{9–13} The signature optical property of these nanoparticles is the localized surface plasmon resonance (LSPR). The LSPR occurs under conditions where the frequency of photons incident on the nanoparticle is resonant with the collective excitation of its conduction electrons. Excitation of the LSPR is characterized by strong, wavelength-selective extinction¹⁴ and enhanced electromagnetic fields at the nanoparticle surface.¹² It is this field enhancement that is responsible for the observation of all surface-enhanced spectroscopies, and it is the basis for the electromagnetic (EM) enhancement mechanism, which is used to account for the large enhancement in scattering intensity relative to what it would be in the absence of a surface. Surface-enhanced Raman scattering (SERS) is characterized by typical enhancements of 10^6 in the Raman cross section of analytes bound to nanoscale noble metal features, and reports in 1997 of single-molecule detection using SERS have rejuvenated interest in this analytical technique.^{15,16} It is generally accepted that the electromagnetic mechanism of SERS accounts for the majority of the enhancement factors (EF) typically observed; however, a clear understanding of the mechanism responsible for the 10^{14} – 10^{15} enhancement required for the detection of single molecules remains elusive.

Surface-enhanced Raman excitation spectroscopy (SERES) can provide key insights into the mechanism of SERS and could facilitate the understanding of the single-molecule SERS (SM-SERS) phenomenon. Detailed comparison of SERES profiles with the LSPR spectra of SERS substrates could further

substantiate the validity of the EM mechanism and possibly uncover the optical properties of electromagnetic hot spots in nanoparticle aggregates that are hypothesized to be responsible for SMSERS.^{17,18} Even though SERES has the potential to improve the understanding of SERS, less than one percent of SERS literature has focused on this topic. The lack of SERES literature is primarily due to the difficulty of performing a SERES experiment, which generally requires a broadly tunable laser source for excitation and a three-stage spectrometer for efficient rejection of Rayleigh scattered light.

Wavelength-scanned SERES (WS SERES) involves the measurement of SERS enhancement for several laser excitation wavelengths, λ_{ex} . This technique was recognized as a useful tool for probing the EM mechanism immediately following the discovery of SERS. An obvious limitation of this technique is that the number of data points is determined by the tunability of the excitation laser and detection system. These substantial instrumental requirements have led to the majority of SERES publications suffering from low data point density and/or limited spectral coverage.^{19–23} These limitations prevent the establishment of conclusive generalizations from SERES data. Additionally, most SERES experiments have been performed using surface-enhancing substrates with an unknown or poorly characterized distribution of roughness features. In the few cases where the surfaces are carefully characterized, it is shown that there is a wide distribution of roughness feature sizes.^{23,24} Other studies do not include characterization of the LSPR of the substrate,^{19,20} which prevents any direct comparison of the excitation profiles to the spectral location of the LSPR λ_{max} . The most common substrates historically employed in SERES experiments are Ag island films and Ag colloidal solutions. In these cases, the majority of the SERS excitation profiles peak at excitation wavelengths ($\lambda_{\text{ex,max}}$) near 500–600 nm.^{24–28} The peaks of the excitation profiles have been shown to shift to the red with increased aggregation,^{22,24,26,27} which is a qualitative

* To whom correspondence should be addressed. E-mail: vanduyne@chem.northwestern.edu.

[†] These authors contributed equally to this work.

result predicted by the EM mechanism. With these substrates it is difficult to make a direct comparison between the LSPR of the substrate and the SERS excitation profile because the LSPR of the substrate is a superposition of a wide variety of LSPR wavelengths corresponding to the different roughness features.

Two exceptions to the above statements regarding roughness features are the well-known experiments by Liao and co-workers on microlithographically prepared Ag posts²⁹ and recent work by Felidj and co-workers on e-beam lithographically produced arrays of gold elongated nanoparticles.²¹ The former groundbreaking work demonstrated excitation profiles where $\lambda_{\text{ex,max}}$ shifts to the red with increased particle aspect ratio and with increased dielectric constant of the medium surrounding the particles. These results qualitatively agree with the EM mechanism, but the LSPR of these substrates was not measured for a direct comparison. In the latter work, the SERS enhancement was shown to peak at halfway between the excitation wavelength and the wavelength of the Raman scattered photon. This important experiment was the first observation of precisely what is predicted by the EM mechanism. Unfortunately, this result was only obtained on one sample with a profile consisting of only three data points.

The limitation of laser and detection tunability has been circumvented by several researchers using a unique approach that involves investigating substrates with variations in the spectral location of the LSPR λ_{max} .^{30–32} These variations allow investigation of the relationship between the LSPR and SERS enhancement using a single excitation wavelength. Our previous work using plasmon-sampled SERES (PS SERES) on well-defined arrays of nanoparticles was the first systematic study using this technique. The conclusion of that study was that the condition for maximum enhancement occurred when the peak extinction wavelength of the LSPR, λ_{max} , is located between λ_{ex} and the wavelength that is Raman-scattered by the analyte molecules, λ_{vib} . This conclusion supports the EM mechanism, which predicts that maximum SERS intensity is achieved when the LSPR strongly enhances both the incident and scattered photon intensities. However, because of inefficient detection of the Raman scattering, EFs could only be measured down to 1 order of magnitude lower than the peak enhancement. In addition, while this work represented a significant step forward in SERES, the noise levels prevented drawing detailed conclusions from the data.

The work presented herein utilizes a broadly tunable Raman system to measure excitation profiles with the greatest number of data points ever achieved in a WS SERES experiment. A broadly tunable laser system, a versatile detection system, and a well-characterized surface-enhancing substrate are all employed in order to overcome the traditional shortcomings of WS SERES experiments. The use of a CW-modelocked Ti:Sapphire and its harmonics allow for continuous tunability over the spectral ranges 350–500 and 700–1000 nm. The visible region not covered by the Ti:Sapphire system was augmented with the use of a solid-state laser and a tunable dye laser. A triple spectrograph equipped with a CCD camera allows for rapid, multichannel spectral acquisition with efficient rejection of Rayleigh-scattered photons. The SERS substrates used in this work are triangular nanoparticle arrays fabricated by nanosphere lithography (NSL). These substrates have been well characterized by previous work.^{14,33,34} They present a significant advantage over many of the traditional SERS substrates for SERES studies because NSL-fabricated triangular nanoparticles exhibit extremely narrow size distributions, making them an indispen-

sable tool for probing the fundamental characteristics of SERS. Tunability of the LSPR λ_{max} of these nanoparticles throughout the visible and NIR wavelengths can be achieved by systematically varying the dimension of the nanoparticles.¹⁴ Even though the surface coverage of these nanoparticles is $\sim 7\%$, strong SERS intensities are observed from analytes adsorbed to these substrates due to the strong enhancement ($\text{EF} \sim 10^8$, vide infra) NSL-fabricated arrays exhibit.³⁰

The present work demonstrates the most detailed set of WS SERES experiments ever performed on optically and topographically characterized SERS substrates. The relative SERS enhancement of these substrates has been shown to vary by 3 orders of magnitude over the spectral range investigated. It is worth noting that this is not a study on the practical application of SERS for chemical analysis. Factors such as spectrograph throughput, detector efficiency, and the ν^4 scattering dependence of Raman photons play an important role in the practice of Raman spectroscopy. Instead, this study seeks to contribute fundamental insights into the origins of the SERS effect and to test various aspects of the EM mechanism not previously studied. This work demonstrates that for substrates with LSPR λ_{max} values throughout the visible spectrum, the maximum SERS enhancement consistently occurs at excitation wavelengths slightly shorter than the LSPR λ_{max} , such that both the incident photon and the Raman scattered photon are strongly enhanced. The largest EF measured was $\sim 10^8$ for NSL-fabricated nanoparticles, which is consistent with values previously reported using these substrates.

Experimental Methods

Materials. Glass substrates (18-mm diameter, No. 1 coverslips) and cyclohexane were purchased from Fisher Scientific (Hampton, NH). Silicon(111) was purchased from Silicon Quest International (Santa Clara, CA) and cut into $\sim 1.5 \times 1.5$ -cm pieces. Pretreatment of substrates utilized H_2SO_4 , H_2O_2 , and NH_4OH , which were purchased from Fisher Scientific (Pittsburgh, PA). Benzenethiol was purchased from Aldrich (Milwaukee, WI) and used as received. Surfactant-free white carboxyl-substituted polystyrene latex nanospheres were obtained from Interfacial Dynamics (Portland, OR). Ag (99.99%, 0.04-in. diameter) was purchased from D. F. Goldsmith (Evanston, IL), and tungsten vapor deposition boats were purchased from R. D. Mathis (Long Beach, CA). For all steps of substrate preparation, ultrapure water ($18.2 \text{ M}\Omega \text{ cm}^{-1}$) from a Millipore academic system (Marlborough, MA) was used.

Preparation of Nanoparticle Samples. The glass coverslips (for triangular nanoparticle fabrication) used as substrates were pretreated in two steps: (1) piranha etch, 3:1 $\text{H}_2\text{SO}_4/30\% \text{ H}_2\text{O}_2$ at 80 °C for 1 h, to clean the substrate, and (2) base treatment, 5:1:1 $\text{H}_2\text{O}/\text{NH}_4\text{OH}/30\% \text{ H}_2\text{O}_2$ with sonication for 1 h, to render the surface hydrophilic. After pretreatment of the substrates, 2–3 μL of undiluted nanosphere solution was drop-coated onto the substrates. The substrates were then allowed to dry under ambient conditions, resulting in large areas of close-packed monolayers of nanospheres. Metal films were deposited onto the substrates in a modified Consolidated Vacuum Corporation vapor deposition system with a base pressure of 10^{-7} Torr. Deposition rate and mass thickness were measured using a Leybold Inficon XTM/2 quartz crystal microbalance. The nanospheres were removed from the substrate after the metal deposition by sonicating the samples in ethanol for 5 min. Before the SERS experiments, the samples were incubated in 1 mM benzenethiol in methanol for > 3 h and then rinsed with methanol.

SERES Instrumentation. Figure 1 shows a schematic of the instrumentation used for the SERES experiments. All optical

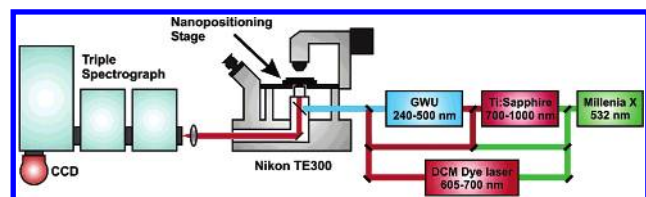


Figure 1. Schematic diagram of the WS SERES apparatus.

measurements were performed using a Nikon Eclipse TE300 inverted microscope (Fryer Co., Huntley, IL) equipped with a 20 \times objective (NA = 0.5). Substrates were mounted on a piezoelectric stage (model P-517.3CD, Polytech PI, Auburn, MA) to allow for sample positioning and raster-scanning during spectral acquisition. The light scattered by the samples was analyzed with a TriplePro three-stage spectrograph equipped with a liquid nitrogen-cooled, deep-depletion Spec-10:400BR CCD detector (Roper Scientific, Trenton, NJ). A color video camera was also attached to the front port of the microscope to facilitate laser alignment and positioning of the samples. Laser excitation was provided by the following systems: (1) a Spectra-Physics (Mountain View, CA) Millennia Xs (λ_{ex} = 532 nm), (2) a Spectra-Physics Tsunami with GWU harmonic generator (λ_{ex} = 350–500, 700–1000 nm), and (3) a Coherent (Santa Clara, CA) model 590 dye laser (λ_{ex} = 610–700 nm). The laser light from the tunable laser systems was filtered using Pellin-Broca prisms or a diffraction grating to ensure monochromatic illumination of the sample. For the NSL-fabricated triangular nanoparticles, in-situ measurement of the LSPR spectrum was achieved by illuminating the sample with the microscope lamp and analyzing the transmitted light with a fiber-optically coupled miniature spectrometer (model SD2000, Ocean Optics, Dunedin, FL). Atomic force micrographs of the SERS substrates were collected in noncontact mode using a Molecular Imaging (Tempe, AZ) PicoPlus microscope.

SERES Methods. During spectral acquisition, the substrates were linearly scanned over a range of 100 μm at a rate of 2 Hz to prevent sample degradation. It is worthwhile to note that all illumination powers reported in this work were the laser powers incident on the microscope beam splitter, not the power incident on the sample. On the basis of experimental measurements, approximately 5–10% of the reported power is incident on the sample; however, because of the intensity standard the absolute power at the sample is not a critical measurement.

To correct for any variation of the SERS intensity not due to the enhancement by the substrate, the 1444 cm^{-1} normal Raman scattering band of neat cyclohexane was used as an intensity standard. This standard was used to correct for the inherent ν^4 behavior of Raman scattering, spectral dependence of the detection system, and differences in the illumination power. This was accomplished by mounting each sample face down as the bottom window of a transparent flow cell. When the flow cell was filled with cyclohexane, the nanoparticle array with an adsorbed benzenethiol monolayer was not in contact with the cyclohexane liquid. In this way, following each SERS acquisition, an intensity standard spectrum of cyclohexane could be taken by translating the inverted microscope objective ~ 400 μm vertically. A schematic depiction of this setup is shown in Figure 2.

Results and Discussion

WS SERES Results. A representative SERS spectrum of benzenethiol on a Ag nanoparticle array is shown in Figure 3. An AFM image of the sample from which this spectrum was taken is shown in the inset. This array was fabricated by

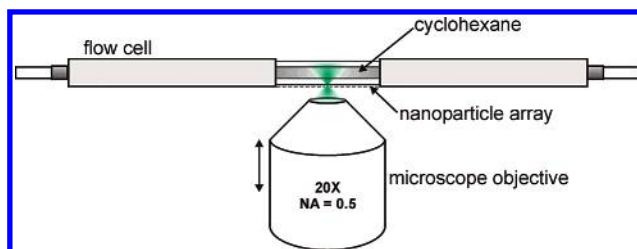


Figure 2. Schematic diagram of flow cell containing cyclohexane for intensity standard measurements.

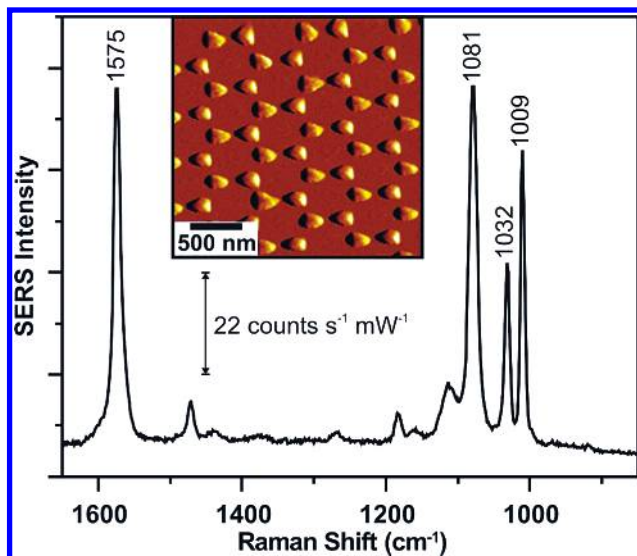


Figure 3. Representative SERS spectrum of benzenethiol-dosed NSL substrate. λ_{ex} = 620 nm, P = 3.0 mW, acquisition time = 150 s. An atomic force micrograph of the sample is shown in the inset.

depositing 55 nm of Ag through a mask formed with 450 nm diameter nanospheres. Figure 4 shows four excitation profiles for the 1575 cm^{-1} peak of benzenethiol, each with an LSPR λ_{max} at a distinctly different location. The SERES profile in Figure 4A consists of 13 data points measured over the spectral range 420–500 nm. Because the formation of a monolayer of benzenethiol on these nanoparticle arrays results in a significant red shift in the position of the LSPR λ_{max} , it was necessary to anneal this sample under vacuum at 300 $^{\circ}\text{C}$ for 1 h prior to benzenethiol addition in order to achieve a final LSPR λ_{max} at a wavelength shorter than 500 nm. It has been previously shown that annealing NSL-derived samples results in a large blue shift of the LSPR due to changing the shape of the nanoparticles.¹⁴ The LSPR λ_{max} of this substrate was measured to be 489 nm (20450 cm^{-1}). The largest SERS enhancement occurs at λ_{ex} = 485 nm. Fitting a Gaussian line shape to the data reveals that the peak of the excitation profile, $\lambda_{\text{ex,max}}$, is 480 nm (20833 cm^{-1}). The peak enhancement factor (EF) value for this sample was calculated to be 5.5×10^5 . This value is low in comparison to the values determined for the other samples because the shape of the nanoparticles is made more ellipsoidal by annealing. In addition to shifting the LSPR λ_{max} to shorter wavelengths, this change decreases the intensity of the electromagnetic fields at the nanoparticle surfaces.

The SERES profile in Figure 4B consists of 14 data points measured over the spectral range 532–690 nm. The LSPR λ_{max} of this substrate was measured to be 663 nm (15083 cm^{-1}). The largest SERS enhancement occurs for λ_{ex} = 625 nm. The maximum of a Gaussian line shape fit to the data is 625 nm (16000 cm^{-1}). The peak EF value for this sample is 1.2×10^7 . The SERES profile in Figure 4C consists of 15 data points measured over the spectral range 532–740 nm. The LSPR λ_{max}

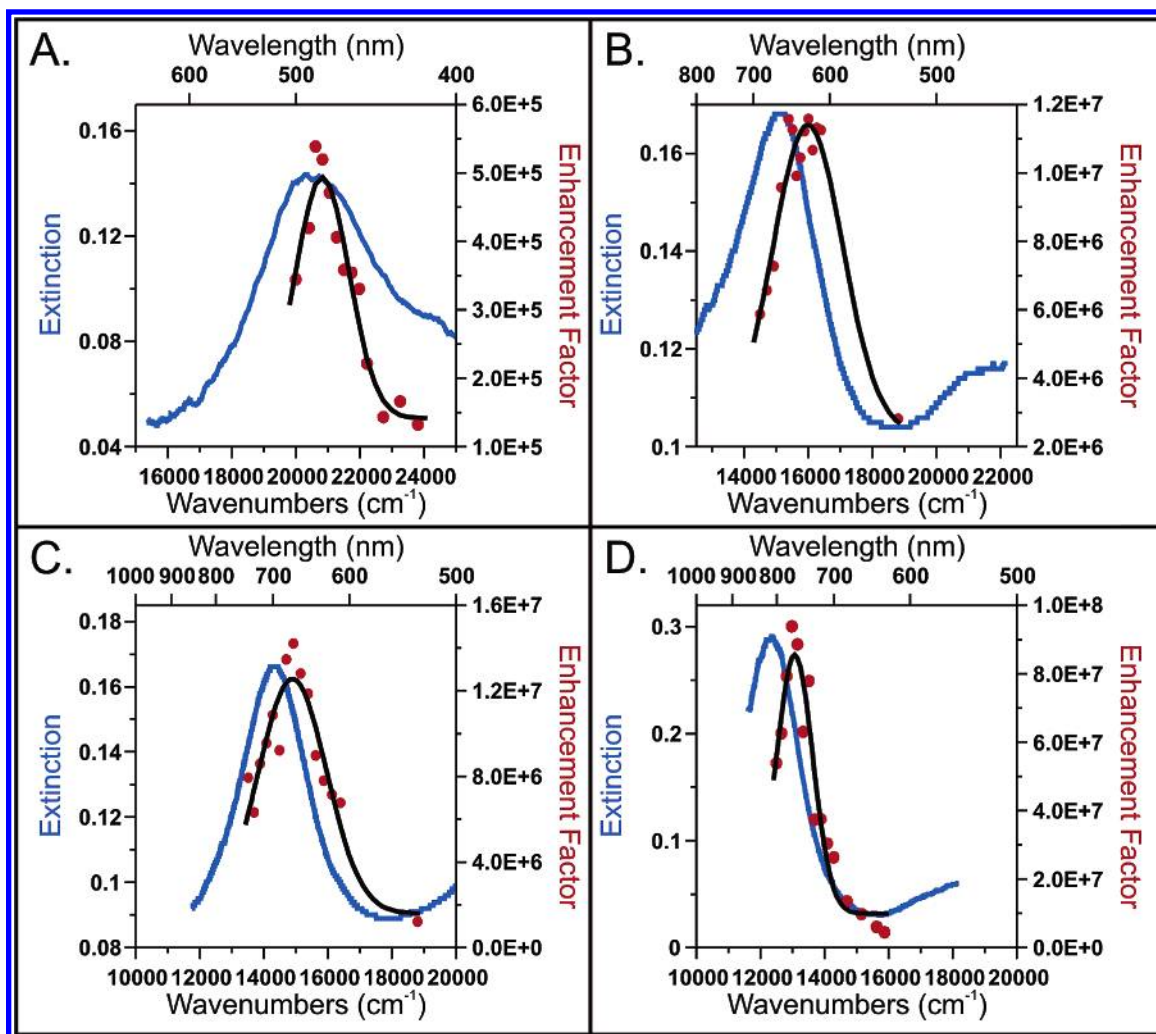


Figure 4. Surface-enhanced Raman excitation spectra of the 1575 cm^{-1} peak of benzenethiol with cyclohexane as intensity standard. (A) Substrate annealed at $300\text{ }^{\circ}\text{C}$ for 1 h. LSPR $\lambda_{\text{max}} = 489\text{ nm}$, profile fit maximum at $\lambda_{\text{ex,max}} = 480\text{ nm}$. (B) LSPR $\lambda_{\text{max}} = 663\text{ nm}$, profile fit maximum at $\lambda_{\text{ex,max}} = 625\text{ nm}$. (C) LSPR $\lambda_{\text{max}} = 699\text{ nm}$, profile fit maximum at $\lambda_{\text{ex,max}} = 671\text{ nm}$. (D) LSPR $\lambda_{\text{max}} = 810\text{ nm}$, profile fit maximum at $\lambda_{\text{ex,max}} = 765\text{ nm}$.

of this substrate was measured to be 699 nm (14306 cm^{-1}). The largest SERS enhancement occurs for $\lambda_{\text{ex}} = 670\text{ nm}$. The maximum of a Gaussian line shape fit to the data is 671 nm (14903 cm^{-1}). The peak EF value for this sample is 1.4×10^7 . The SERES profile in Figure 4D consists of 15 data points measured over the spectral range $630\text{--}800\text{ nm}$. The LSPR λ_{max} of this substrate was measured to be 810 nm (12346 cm^{-1}). The largest SERS enhancement occurs for $\lambda_{\text{ex}} = 770\text{ nm}$. The maximum of a Gaussian line shape fit to the data is 765 nm (13072 cm^{-1}). The peak EF value for this sample is 9.3×10^7 .

To verify that this behavior can be generalized, two SERES experiments were undertaken in which a different benzenethiol band (1081 cm^{-1}) and intensity standard were monitored. In this case, the intensity standard was the 520 cm^{-1} phonon mode of silicon. The wavelength-dependent absorptivity of silicon requires that the measured Raman intensities must be corrected for differences in laser penetration depth. The penetration depth was calculated at all of the excitation wavelengths using the silicon absorptivities measured by Aspnes and Studna.³⁵ The silicon spectra were then normalized so that the intensities were representative of equivalent probe volumes. In addition, a correction was performed to account for the fact that the 520 cm^{-1} band of Si scatters at a significantly different wavelength than the 1081 cm^{-1} band of benzenethiol, particularly at redder excitation wavelengths. No correction was performed to account

for variation in the Raman scattering cross section of silicon because over the range of excitation wavelengths utilized in this work, the differences in the experimentally determined values of the polarizability of silicon are negligible.³⁶ The excitation spectra are shown in Figure 5. The SERES profile in Figure 5A consists of 13 data points measured over the spectral range $475\text{--}700\text{ nm}$. The LSPR λ_{max} of this substrate was measured to be 690 nm (14493 cm^{-1}). The largest SERS enhancement occurs for $\lambda_{\text{ex}} = 660\text{ nm}$. The maximum of a Gaussian line shape fit to the data is 662 nm (15106 cm^{-1}). The peak EF value for this sample is 1.9×10^7 . The SERES profile in Figure 5B consists of 17 data points measured over the spectral range $630\text{--}790\text{ nm}$. The LSPR λ_{max} of this substrate was measured to be 744 nm (13441 cm^{-1}). The largest relative SERS intensity occurs for $\lambda_{\text{ex}} = 700\text{ nm}$. The maximum of a Gaussian line shape fit to the data is 715 nm (13986 cm^{-1}). The peak EF value for this sample is 1.8×10^7 .

Each substrate exhibits a SERES profile that has a similar line shape to the extinction spectrum of the substrate. Also, the $\lambda_{\text{ex,max}}$ for the NSL-fabricated substrates is consistently shorter than the LSPR λ_{max} . In all cases, the maximum SERS enhancement occurs when the substrate LSPR λ_{max} is located between λ_{ex} and λ_{vib} . Under these conditions, both the incident and scattered photons experience enhancement by the LSPR. These

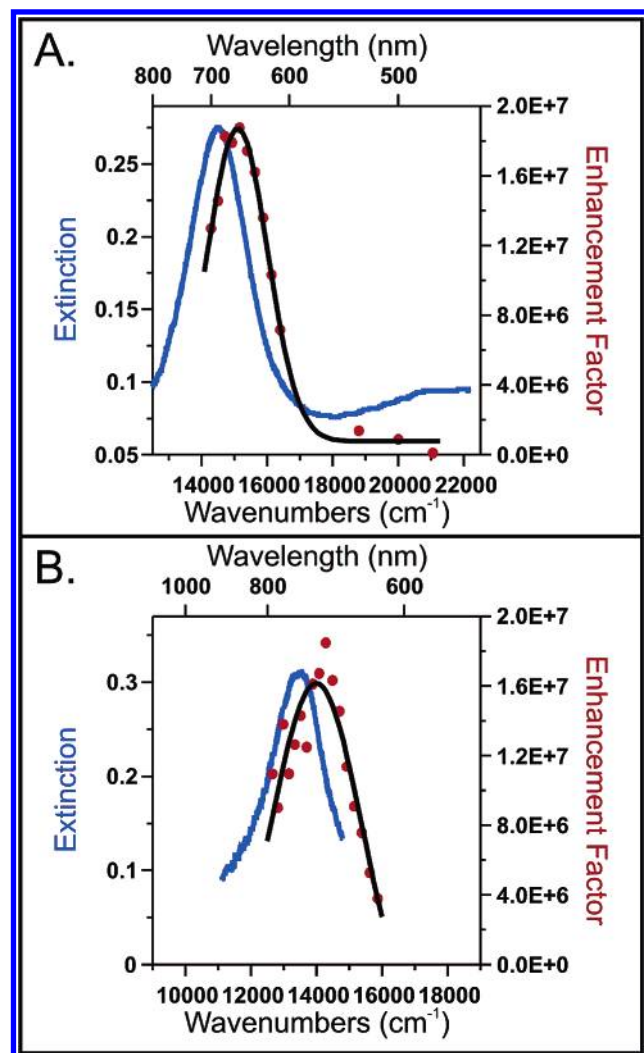


Figure 5. Surface-enhanced Raman excitation spectra of the 1081 cm⁻¹ peak of benzenethiol with Si as intensity standard. (A) LSPR λ_{max} = 690 nm, profile fit maximum at $\lambda_{\text{ex,max}}$ = 662 nm. (B) LSPR λ_{max} = 744 nm, profile fit maximum at $\lambda_{\text{ex,max}}$ = 715 nm.

data are in accordance with the EM mechanism of SERS and the experimental work performed previously using PS SERES.

If the peak in the SERS enhancement occurs when the LSPR λ_{max} of the sample is equal to $(\lambda_{\text{ex}} + \lambda_{\text{vib}})/2$, then $\lambda_{\text{ex,max}}$ should be different for the various Raman bands of benzenethiol on a single sample. It is expected that $\lambda_{\text{ex,max}}$ will have a larger separation from the LSPR λ_{max} for a large Raman shift than for a small shift. Excitation profiles for three benzenethiol peaks on a single substrate are shown in Figure 6. For this substrate, the LSPR λ_{max} is 729 nm. Figure 6A shows the SERS excitation profile for the 1575 cm⁻¹ peak of benzenethiol, normalized to the 1444 cm⁻¹ peak of liquid cyclohexane. The separation in wavenumbers between the LSPR λ_{max} and $\lambda_{\text{ex,max}}$ is 734 cm⁻¹. In Figure 6B, the excitation profile for the 1081 cm⁻¹ benzenethiol peak (normalized to the 1028 cm⁻¹ peak of cyclohexane) is shown. The separation in wavenumbers between the LSPR λ_{max} and $\lambda_{\text{ex,max}}$ is 569 cm⁻¹. Finally, in Figure 6C, the excitation profile for the 1009 cm⁻¹ benzenethiol peak (normalized to the 1028 cm⁻¹ peak of cyclohexane) is shown, and the separation in wavenumbers between the LSPR λ_{max} and $\lambda_{\text{ex,max}}$ is 488 cm⁻¹. These data demonstrate the qualitative trend whereby the $\lambda_{\text{ex,max}}$ in the excitation spectra of larger Raman shifted bands yield a larger separation from the LSPR λ_{max} than those of smaller Raman shifted bands, and this once again lends support to the EM mechanism.

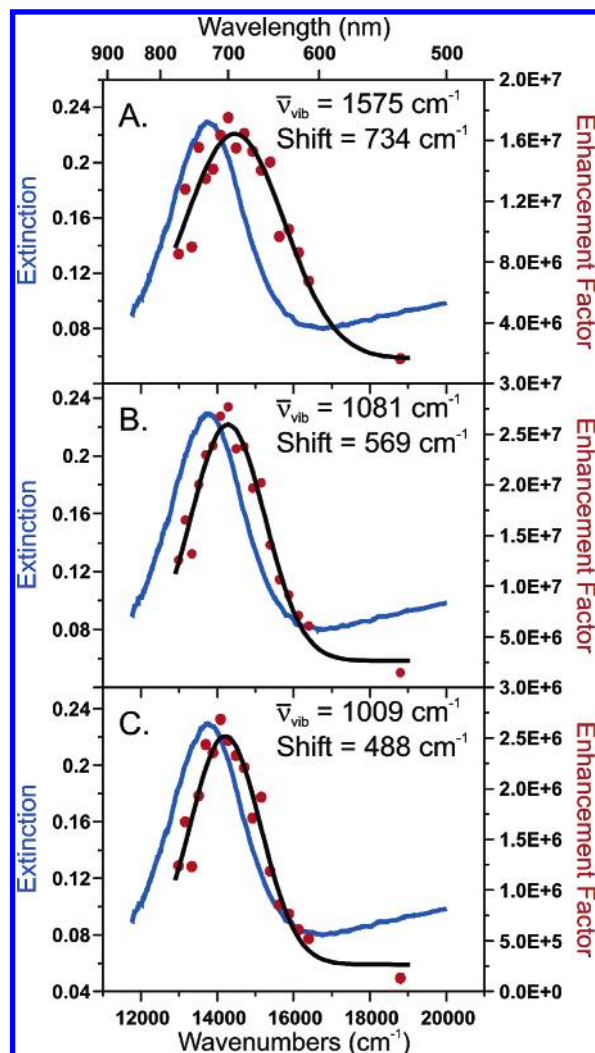


Figure 6. Effect of Stokes Raman shift. (A) Profile of the 1575 cm⁻¹ vibrational mode of benzenethiol. Distance between LSPR λ_{max} and excitation profile fit line $\lambda_{\text{ex,max}}$ = 734 cm⁻¹. EF = 1.8×10^7 . (B) 1081 cm⁻¹ vibrational mode, shift = 569 cm⁻¹, EF = 2.8×10^7 . (C) 1009 cm⁻¹ vibrational mode, shift = 488 cm⁻¹, EF = 2.7×10^6 .

Previous work has demonstrated that the spectral location of the LSPR is sensitive to the presence of molecular adsorbates.^{1,4,37} Therefore, it is important to note that the relationship between the LSPR spectra and SERES profiles depicted in Figures 4–6 pertains to LSPR spectra measured after adsorption of the analyte molecule. Figure 7 demonstrates the importance of considering this point. For a bare nanoparticle array, the LSPR λ_{max} was measured to be 672 nm. After incubation in 1 mM benzenethiol for >3 h, thorough rinsing with methanol, and drying, the LSPR λ_{max} was observed to have red-shifted by 57 nm to 729 nm. Measurement of the WS SERES profile yields $\lambda_{\text{ex,max}}$ = 692 nm. This is blue-shifted with respect to the LSPR λ_{max} of the adsorbate-covered sample, as observed for the other samples used in this study, but red-shifted with respect to the LSPR λ_{max} of the bare nanoparticle array. This demonstrates that it is critical to characterize the LSPR of a SERS substrate after analyte adsorption in order to choose the appropriate laser excitation wavelength for maximizing EF or to draw any conclusions about the fundamental mechanism of the SERS effect.

SERS Enhancement Factor Calculation. SERS EF values were calculated by comparing the intensity of the appropriate benzenethiol peak (1081 or 1575 cm⁻¹) measured in the SERS experiments to the corresponding peak measured from liquid

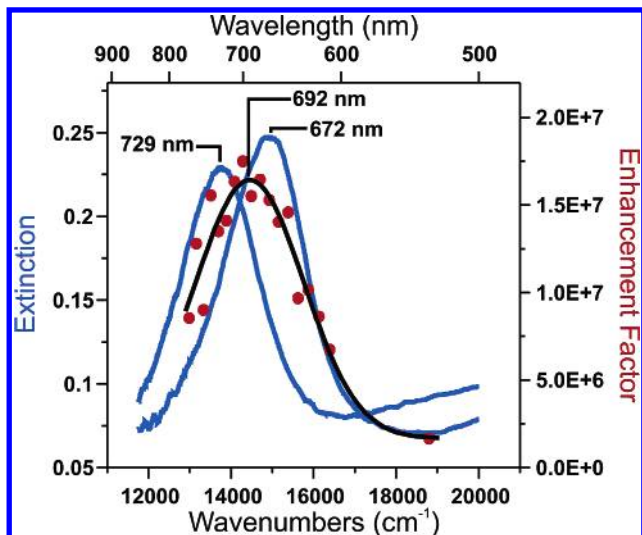


Figure 7. LSPR shift and SERES profile for the 1575 cm^{-1} peak of benzenethiol. The line with $\lambda_{\text{max}} = 672$ nm is the LSPR extinction of the bare nanoparticle array. The line with $\lambda_{\text{max}} = 729$ nm is the LSPR extinction of the nanoparticle array with an adsorbed monolayer of benzenethiol. The line with $\lambda_{\text{ex,max}} = 692$ nm is the best fit to the SERES data points.

benzenethiol. The normal Raman spectrum was measured at $\lambda_{\text{ex}} = 480, 532,$ and 670 nm from a $37\text{ }\mu\text{m}$ -thick cell filled with benzenethiol. When the intensities are normalized for laser power and acquisition time, under the same collection conditions, the SERS EF is given by

$$\text{EF} = \frac{N_{\text{vol}} I_{\text{surf}}}{N_{\text{surf}} I_{\text{vol}}}$$

where N_{vol} and N_{surf} are the number of molecules probed in the liquid sample and on the SERS substrates, respectively, and I_{vol} and I_{surf} are the corresponding normal Raman and SERS intensities. On the basis of scanning silicon knife edge measurements, the beam waist of the $20\times$ objective is $4.0\text{ }\mu\text{m}$ with $\lambda_{\text{ex}} = 532$ nm. Assuming a benzenethiol packing density of 6.8×10^{14} molecules cm^{-2} and the 7.4% surface coverage of nanoparticles, approximately 6.3×10^6 molecules are probed on the triangular nanoparticle array substrates (N_{surf}). For the normal Raman experiment, the probe volume was approximated as a cylinder with a radius of $2.0\text{ }\mu\text{m}$ and a height of $37\text{ }\mu\text{m}$, resulting in 2.7×10^{12} molecules being probed (N_{vol}). The values for N_{surf} and N_{vol} , along with the SERS intensities for the 1081 and 1575 cm^{-1} peaks (measured with one of the excitation wavelengths listed above), were substituted into the above equation to calculate the EFs. The peak EF values were calculated by compensating for the differences in the relative SERS intensity measured at $\lambda_{\text{ex,max}}$ versus an excitation wavelength at which a liquid benzenethiol spectrum was measured. Figure 8 shows the spectra necessary for calculating the peak EF for a single SERES profile. This example pertains to the spectrum where $\lambda_{\text{max}} = 810$ nm and $\lambda_{\text{ex,max}} = 765$ nm (Figure 4D). Figure 8A shows the SERS spectrum of benzenethiol on a nanoparticle array taken at $\lambda_{\text{ex}} = 670$ nm. The 1575 cm^{-1} peak intensity is $22.9\text{ ADU s}^{-1}\text{ mW}^{-1}$ (I_{surf}). Figure 8B shows the normal Raman spectrum of benzenethiol in the $37.0\text{ }\mu\text{m}$ -thick cell at $\lambda_{\text{ex}} = 670$ nm. The 1575 cm^{-1} peak intensity is $0.792\text{ ADU s}^{-1}\text{ mW}^{-1}$ (I_{vol}). When substituted into the EF equation, these values yield an EF of 1.24×10^7 . This EF is for $\lambda_{\text{ex}} = 670$, but because the maximum normalized SERS intensity for this profile was $\lambda_{\text{ex}} = 770$ nm, this value needs to be multiplied by an appropriate

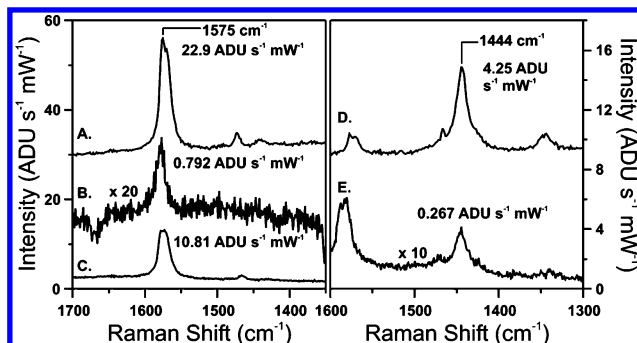


Figure 8. Example of EF calculation. (A) SERS spectrum of benzenethiol on a nanoparticle array at $\lambda_{\text{ex}} = 670$ nm. (B) Raman spectrum of neat benzenethiol at $\lambda_{\text{ex}} = 670$ nm. (C) SERS spectrum of benzenethiol on the same sample as (A) at $\lambda_{\text{ex}} = 770$ nm (the peak of the excitation profile). (D) Raman spectrum of cyclohexane at $\lambda_{\text{ex}} = 670$ nm. (E) Raman spectrum of cyclohexane at $\lambda_{\text{ex}} = 770$ nm.

scale factor to calculate the peak EF. The normalized SERS intensity at $\lambda_{\text{ex}} = 670$ nm is calculated by dividing the SERS intensity of the 1575 cm^{-1} benzenethiol peak in Figure 8A ($22.9\text{ ADU s}^{-1}\text{ mW}^{-1}$) by the normal Raman intensity of the 1444 cm^{-1} peak of cyclohexane at the same excitation wavelength, Figure 8D ($4.25\text{ ADU s}^{-1}\text{ mW}^{-1}$), yielding a relative intensity of 5.39. The normalized SERS intensity at $\lambda_{\text{ex}} = 770$ nm is calculated by dividing the intensity in Figure 8C ($10.8\text{ ADU s}^{-1}\text{ mW}^{-1}$) by that in Figure 8E ($0.267\text{ ADU s}^{-1}\text{ mW}^{-1}$), which yields a relative intensity of 40.4. Therefore, the normalized SERS intensity at $\lambda_{\text{ex}} = 770$ nm is larger than that at $\lambda_{\text{ex}} = 670$ by a factor of $40.4/5.39 = 7.50$. Multiplying the EF value at $\lambda_{\text{ex}} = 670$ by this factor yields a peak EF of 9.3×10^7 . This value, the largest peak EF in this study, was measured from the substrate with the longest-wavelength LSPR λ_{max} . The values for EF reported in this paper are conservative estimates because the probe volume assumed for the normal Raman experiment is likely to be an underestimation of the actual value. Also, the calculated number of adsorbate molecules is most likely an overestimation because the calculation assumes perfect array formation. The nanoparticle arrays contain a small number of defects, which can be assumed to contribute little to the observed characteristics of the SERES profiles. If Raman scattering from the defects were contributing significantly, it is unlikely that the systematic trends demonstrated by this work would be observed. Even with consideration of these points, the peak EF calculated for the triangular nanoparticle arrays is consistent with the average values reported in other experimental work using these same substrates³⁰ and theoretical modeling of triangular Ag nanoparticles.³⁸

Conclusions

This work demonstrates the most thorough WS SERES experiments ever performed on optically and topographically characterized SERS substrates. The experimental apparatus utilized has proven effective for the measurement of relative SERS enhancements that vary by 3 orders of magnitude. This work demonstrates that the relationship between the substrate LSPR and the SERES profile for size-homogeneous nanoparticles is consistent throughout the visible range. In all cases, the experimentally observed behavior is consistent with that predicted by the EM mechanism. Specifically, the strongest SERS enhancement occurs under conditions where the incident and Raman scattered photons are both strongly enhanced. The largest EF measured was $\sim 10^8$ for the triangular nanoparticle arrays studied. Ultimately, refinement of the experimental

apparatus and optimization of SERS enhancement will allow SERES to be performed using single nanoparticle substrates. This level provides the best possible case in terms of reducing sample heterogeneity. These experiments are expected to provide key information to validate the EM mechanism of SERS and will present an additional technique that can be used to study the SMSERS effect.

Acknowledgment. The authors gratefully acknowledge support from the Air Force Office of Scientific Research MURI program (Grant F49620-02-1-0381) and the National Science Foundation (EEC-0118025, DMR-0076097, CHE-0414554, DGE-0114429).

References and Notes

- (1) McFarland, A. D.; Van Duyne, R. P. *Nano Lett.* **2003**, *3*, 1057–1062.
- (2) Kim, Y.; Johnson, R. C.; Hupp, J. T. *Nano Lett.* **2001**, *1*, 165–167.
- (3) Haes, A. J.; Stuart, D. A.; Nie, S.; Van Duyne, R. P. *J. Fluoresc.* **2004**, *14*, 355–367.
- (4) Malinsky, M. D.; Kelly, K. L.; Schatz, G. C.; Van Duyne, R. P. *J. Am. Chem. Soc.* **2001**, *123*, 1471–1482.
- (5) Riboh, J. C.; Haes, A. J.; McFarland, A. D.; Yonzon, C. R.; Van Duyne, R. P. *J. Phys. Chem. B* **2003**, *107*, 1772–1780.
- (6) Flaugh, P. L.; O'Donnell, S. E.; Asher, S. A. *Appl. Spectrosc.* **1984**, *38*, 847–850.
- (7) Asher, S. A.; Chang, S.-Y.; Tse, A.; Liu, L.; Pan, G.; Wu, Z.; Li, P. *Mater. Res. Soc. Symp. Proc.* **1995**, *374*, 305–310.
- (8) Lidorikis, E.; Li, Q.; Soukoulis, C. M. *Phys. Rev. E* **1997**, *55*, 3613–3618.
- (9) Zou, S.; Williams, C. T.; Chen, E. K. Y.; Weaver, M. J. *J. Am. Chem. Soc.* **1998**, *120*, 3811–3812.
- (10) Pipino, A. C. R.; Schatz, G. C.; Van Duyne, R. P. *Phys. Rev. B* **1994**, *49*, 8320–8330.
- (11) Yang, W.-H.; Hulteen, J.; Schatz, G. C.; Van Duyne, R. P. *J. Chem. Phys.* **1996**, *104*, 4313–4323.
- (12) Schatz, G. C.; Van Duyne, R. P. Electromagnetic Mechanism of Surface-Enhanced Spectroscopy. In *Handbook of Vibrational Spectroscopy*; Chalmers, J. M., Griffiths, P. R., Eds.; Wiley: New York, 2002; Vol. 1, pp 759–774.
- (13) Schmidt, J. P.; Cross, S. E.; Buratto, S. K. *J. Chem. Phys.* **2004**, *121*, 10657–10659.
- (14) Jensen, T. R.; Malinsky, M. D.; Haynes, C. L.; Van Duyne, R. P. *J. Phys. Chem. B* **2000**, *104*, 10549–10556.
- (15) Nie, S.; Emory, S. R. *Science* **1997**, *275*, 1102–1106.
- (16) Kneipp, K.; Wang, Y.; Kneipp, H.; Perelman, L. T.; Itzkan, I.; Dasari, R. R.; Feld, M. S. *Phys. Rev. Lett.* **1997**, *78*, 1667–1670.
- (17) Michaels, A. M.; Jiang, J.; Brus, L. *J. Phys. Chem. B* **2000**, *104*, 11965–11971.
- (18) Jiang, J.; Bosnick, K.; Maillard, M.; Brus, L. *J. Phys. Chem. B* **2003**, *107*, 9964–9972.
- (19) Vlckova, B.; Gu, X. J.; Moskovits, M. *J. Phys. Chem. B* **1997**, *101*, 1588–1593.
- (20) Gregory, B. W.; Clark, B. K.; Standard, J. M.; Avila, A. *J. Phys. Chem. B* **2001**, *105*, 4684–4689.
- (21) Felidj, N.; Aubard, J.; Levi, G.; Krenn, J. R.; Hohenau, A.; Schider, G.; Leitner, A.; Aussenegg, F. R. *Appl. Phys. Lett.* **2003**, *82*, 3095–3097.
- (22) Blatchford, C. G.; Campbell, J. R.; Creighton, J. A. *Surf. Sci.* **1982**, *120*, 435–455.
- (23) Van Duyne, R. P.; Hulteen, J. C.; Treichel, D. A. *J. Chem. Phys.* **1993**, *99*, 2101–2115.
- (24) Von Raben, K. U.; Chang, R. K.; Laube, B. L.; Barber, P. W. *J. Phys. Chem.* **1984**, *88*, 5290–5296.
- (25) Weitz, D. A.; Garoff, S.; Gramila, T. J. *Opt. Lett.* **1982**, *7*, 168–170.
- (26) Kerker, M.; Siiman, O.; Wang, D. S. *J. Phys. Chem.* **1984**, *88*, 3168–3170.
- (27) Fornasiero, D.; Grieser, F. *J. Chem. Phys.* **1987**, *87*, 3213–3217.
- (28) Feilchenfeld, H.; Siiman, O. *J. Phys. Chem.* **1986**, *90*, 2163–2168.
- (29) Liao, P. F.; Bergman, J. G.; Chemla, D. S.; Wokaun, A.; Melngailis, J.; Hawryluk, A. M.; Economou, N. P. *Chem. Phys. Lett.* **1981**, *82*, 355–359.
- (30) Haynes, C. L.; Van Duyne, R. P. *J. Phys. Chem. B* **2003**, *107*, 7426–7433.
- (31) Weimer, W. A.; Dyer, M. J. *Appl. Phys. Lett.* **2001**, *79*, 3164–3166.
- (32) Oldenburg, S. J.; Westcott, S. L.; Averitt, R. D.; Halas, N. J. *J. Chem. Phys.* **1999**, *111*, 4729–4735.
- (33) Hulteen, J. C.; Treichel, D. A.; Smith, M. T.; Duval, M. L.; Jensen, T. R.; Van Duyne, R. P. *J. Phys. Chem. B* **1999**, *103*, 3854–3863.
- (34) Haynes, C. L.; Van Duyne, R. P. *J. Phys. Chem. B* **2001**, *105*, 5599–5611.
- (35) Aspnes, D. E.; Studna, A. A. *Phys. Rev. B* **1983**, *27*, 985–1009.
- (36) Grimsditch, M.; Cardona, M. *Phys. Status Solidi B* **1980**, *102*, 155–161.
- (37) Haes, A. J.; Van Duyne, R. P. *J. Am. Chem. Soc.* **2002**, *124*, 10596–10604.
- (38) Hao, E.; Schatz, G. C. *J. Chem. Phys.* **2004**, *120*, 357–366.